Available online at www.sciencedirect.com
ScienceDirect
Journal of Organometallic Chemistry 693 (2008) 1850–1856
Journal of Organometallic Chemistry
www.elsevier.com/locate/jorganchem

Metal atom dynamics in organometallics: Cyano ferrocenes

Rolfe H. Herber [a,*], Israel Nowik [a], Jeffrey O. Grosland [b], Ryan G. Hadt [b], Victor N. Nemykin [b,*]

[a] Racah Institute of Physics, The Hebrew University of Jerusalem, 91901 Jerusalem, Israel
[b] Department of Chemistry and Biochemistry, University of Minnesota Duluth, Duluth, MN 55812, USA

Received 4 February 2008; accepted 9 February 2008
Available online 15 February 2008

Abstract

Six structurally related cyano ferrocenes have been examined by temperature-dependent Mössbauer effect spectroscopy (MES) to yield information concerning the isomeric shift (IS), quadrupole splitting (QS), and related parameters characterizing the iron atom in these compounds. The IS is related to the s-electron density at the Fe nucleus, while the QS is related to the symmetry and magnitude of the electrostatic field. In addition, these data can yield information related to the dynamics of the metal atom and are in excellent agreement with X-ray crystal data. Density functional theory (DFT) calculations have been used to obtain values for the three principal components of the electric field gradient tensor as well as the electron density at the metal atom site. The results of the DFT calculations and the MES data are found to be in exceptionally good agreement in these compounds.

Keywords: Cyano ferrocenes; Mössbauer spectroscopy; DFT calculations

1. Introduction

Because of their potential application in switchable molecular optical and electronic nanodevices, ferrocene containing porphyrins and phthalocyanins have been intensively investigated in the recent literature [1]. An improved mercury-free synthesis of the previously poorly characterized tricyanovinyl ferrocene has been reported [2] and its crystal structure has been determined at 173 and 293 K. As has been shown in numerous examples in the recent literature [3–6], temperature-dependent Mössbauer effect spectroscopy (MES) can further help to elucidate the metal atom dynamics in ferrocenoid solids, and the present investigation was undertaken to examine the effect of ring substituent electronic and steric effects on the motional characteristics of the metal atom in a number of closely related cyano ferrocenes.

Among the compounds included in this study are cyano ferrocene [$C_{11}H_9FeN$, **1**], *cis*-1,2-dicyano-1-ferrocenylethylene [$C_{14}H_{10}FeN_2$, **2**], *trans*-1,2-dicyano-1-ferrocenylethylene [$C_{14}H_{10}FeN_2$, **3**], 1,2,2-tricyano-1-ferrocenylethylene [$C_{15}H_9FeN_3$, **4**], *cis*-1-iodo-2-cyano-1-ferrocenylethylene [$C_{13}H_{10}FeIN$, **5**], and *trans*-1-iodo-2-cyano-1-ferrocenylethylene [$C_{13}H_{10}FeIN$, **6**]. A schematic representation of these compounds is summarized in Scheme 1.

2. Experimental

(a) *Synthesis:* compound **1**, for which an improved synthesis has recently been reported by Kivrak and Zora [7], was kindly made available by Prof. Zora, and examined as received. Compound **4** [2] as well as compounds **2**, **3**, **5**, and **6** [8] were prepared using literature methods.

(b) *Mössbauer spectroscopy (MES):* The air stable solids were ground with Pyrex powder and mixed with BN to ensure random crystallite orientation in the subsequent MES measurements, transferred to Perspex

* Corresponding authors. Tel.: +972 2 6584 244; fax: +972 2 6586 347 (R.H. Herber).
E-mail addresses: herber@vms.huji.ac.il (R.H. Herber), vnemykin@d.umn.edu (V.N. Nemykin).

0022-328X/$ - see front matter © 2008 Elsevier B.V. All rights reserved.
doi:10.1016/j.jorganchem.2008.02.010

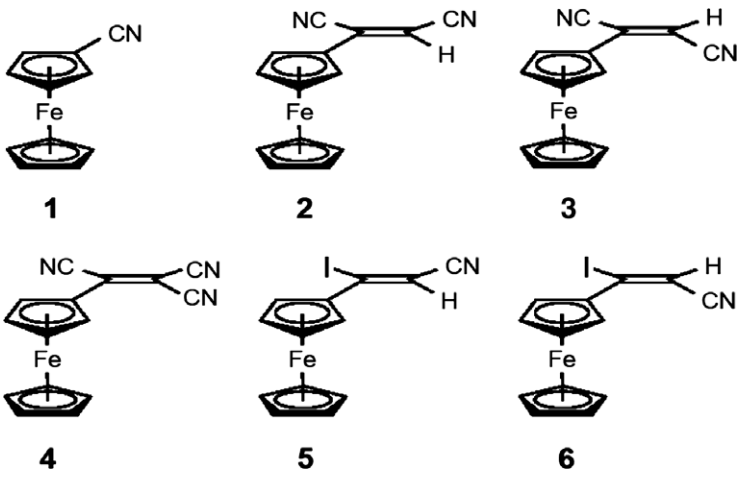

Scheme 1. Representation of the compounds discussed in the text.

sample holders, and mounted in a cryostat in transmission geometry as previously described [3–6]. Spectrometer calibration was effected with α-Fe and all isomer shifts are referred to the centroid of such room temperature calibration spectra. Temperature control over the data sampling intervals (typically 8–36 h) was held to ±0.2° and monitored with the Daswin program as described previously [9].

(c) All DFT calculations were conducted using the GAUSSIAN 03 software package [10] running under either Windows or UNIX OS. In the present investigation, we have used X-ray determined geometries [2,8]. In the case of single point calculations, for all compounds, Becke's pure exchange functional [11] and Perdew and Wang's correlation functional [12] (BPW91) was used. Wachter's original full-electron basis set [13] (contracted as 62111111/3311111/3111) with one set of polarization functions was used for the iron atom, while a 6-311G(d) basis set was employed for all other atoms. In all cases, an ultra fine integral grid with 99 radial shells and 590 angular points per shell along with tight energy (10^{-8} a.u.) SCF convergence criterion has been used.

Electron densities on the ^{57}Fe nuclei in the compounds of interest were calculated using the AIM2000 program [14], which utilizes wavefunctions generated by Gaussian software. Mössbauer quadrupole splittings (ΔE_Q) and asymmetry parameters (η) were calculated using DFT predicted principal components of the electric field gradient tensor (V_{ii}) at the ^{57}Fe nucleus as discussed below.

The isomer shift in Mössbauer spectra arises from differences in the s-electron density at the nucleus in the absorber and a reference compound (typically α-Fe or sodium nitroprusside). It can be calculated using the following equation [15,16]:

$$\delta_{\alpha Fe} = E_A - E_{\alpha Fe} = (2\pi/3)Ze^2([R^2]* - [R^2])(|\Psi(0)|^2_A - |\Psi(0)|^2_{\alpha Fe}) \quad (1)$$

where Z is the atomic number of the nuclei of interest and R and R^* are the average nuclear radii of the ground and excited states of ^{57}Fe, respectively. Due to the fact that $|\Psi(0)|_{\alpha Fe}{}^2$ is constant, the Mössbauer isomer shift can be calculated as [15,16]:

$$\delta_{\alpha Fe} = \alpha[\rho(0) - c] \quad (2)$$

where α, the so-called calibration constant, and $\rho(0)$, the non-relativistic calculated total charge density at the iron nucleus can be easily obtained from a correlation analysis between calculated $\rho(0)$ and experimentally observed $\delta_{\alpha Fe}$ and were taken from a previous study [17].

The quadrupole splitting arises from a non-spherical charge distribution in the $I^* = 3/2$ excited state in the presence of an electric field gradient (EFG) at the ^{57}Fe nucleus. It is related to the components of the electric field gradient as represented by the following equation [15,16]:

$$\Delta E_Q = (1/2)eQV_{zz}\{1 + (\eta^2/3)\}^{1/2} \quad (3)$$

where e is the electron charge and Q being the quadrupole moment of the ^{57}Fe $E = 14.4$ keV excited state. In our case, we used the recently determined value of $Q = 0.16$ (±5%) barn [18], which has been commonly used for the calculation of Mössbauer quadrupole splittings in DFT calculations and is close to the value of 0.158 barn reported recently by Neese's group [19] from the nonrelativistic DFT B3LYP training set. The asymmetry parameter (η) is given by:

$$\eta = (V_{xx} - V_{yy})/V_{zz} \quad (4)$$

where the principle components of the electric field are taken as [14,15]:

$$|V_{zz}| \geqslant |V_{yy}| \geqslant |V_{xx}| \quad (5)$$

3. Results and discussion

With the exceptions noted below, the MES spectra of all of the compounds included in this study consist of well

resolved doublets which can be characterized, *inter alia*, by their isomers shifts (IS), quadrupole splittings (QS), and area under the resonance curve (A). A typical spectrum at 93 K is shown in Fig. 1. For all of the following compounds, the MES parameters at 90 K and derived quantities are summarized in Table 1.

(a) *Compound* **1***:* The IS of this compound is slightly smaller than that reported for the parent unsubstituted ferrocene but quite similar to the other vinyl cyano ferrocenes, *vide infra*. The temperature dependence of the IS is well fitted by a linear regression with a correlation coefficient of 0.997 for 12 data points. The slope, $-(4.007 \pm 0.018) \times 10^{-4}$ mm s^{-1}K^{-1} – permits the calculation of an "effective vibrating mass", M_{eff} [20], of 102 ± 1 Da, and the difference between this value and the "bare" iron atom mass of 57 Da reflects the covalency of the Fe-ring interaction. The area under the resonance curve, A, for an optically "thin" absorber is proportional to the Mössbauer recoil-free fraction, f, where $f = \exp(-\langle x^2_{\text{ave}}\rangle)$, k is the wave vector of the 14.41 keV gamma ray of ^{57}Fe, and $\langle x^2_{\text{ave}}\rangle$ is the mean square amplitude of vibration of the iron atom. For **1**, the temperature dependence of the logarithm of the area under the resonance curve is not well fitted by a linear correlation and shows increasing amplitude of motion at higher temperatures. As pointed out by Gol'danskii and Makarov [21] in the early days of MES, this effect can arise from the fact that the metal atom vibration consists of two contributions: the high frequency vibrations of atoms in molecules and the low frequency vibrations of molecules as a whole. However it should be noted that in ferrocenoid molecular solids there may be ring rotation and librational modes which can contribute to $\langle x^2\rangle$ even at relatively low temperatures. In ferrocene, for example, there are Cp ring modes at 177, 185, and 309 cm^{-1} which are significantly populated above ~200 K. If the high frequency contribution is negligibly small at lower temperatures, and increases at higher temperatures, then the low temperature part can be considered as primarily due to pure molecular vibrations and the low temperature $\langle x^2_{\text{ave}}\rangle$ values can be calculated and extrapolated to higher temperatures. In addition, as has been pointed out by Glidewell et al. [22], in **1** there is a significant hydrogen bonding interaction between N1 of one molecule and atom C21 of an adjacent molecule with C–N distances of 3.381 and 3.384 Å at 294 K. The strength of this interaction will, of course, also be temperature dependent and contribute to the metal atom vibrational amplitudes probed by the MES technique. In the present instance, these contributing factors cannot be separated and hence a calculation of the effective lattice temperature, Θ_{m} [20], cannot reliably be determined from the available data.

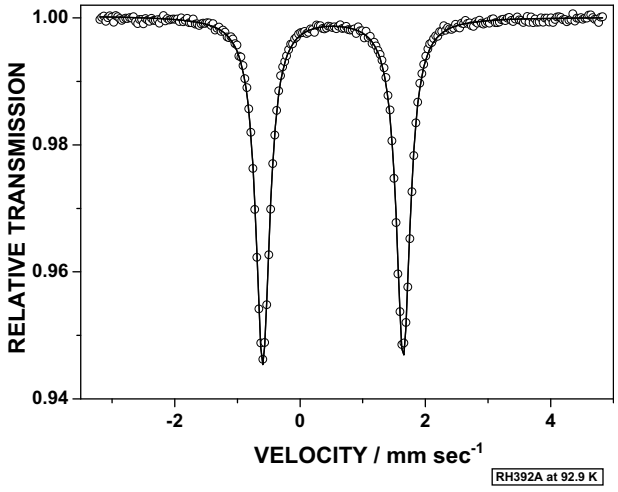

Fig. 1. ^{57}Fe Mössbauer spectrum of **6** at 92.9 K. The velocity scale is with respect to the centroid of an α-Fe absorber spectrum at room temperature.

In the case of **1**, the area ratio R, that is, the area under the more positive velocity peak [A(+)] to that under the more negative velocity peak [A(−)] is found to be essentially temperature independent over the accessible temperature range, $96 < T < 296$ K, indicating the absence of a Gol'danskii-Karyagin [23] effect in this vibration. In other words, in contrast to other ferrocenoids, the vibrational amplitudes parallel and perpendicular to the local symmetry axis running through the cyclopentadienyl ring centers and the metal atom, are essentially equal.

(b) *Compound* **2***:* The hyperfine parameters of **2** are included in the data of Table 1 and are similar to those noted for **1**, including the temperature independence of

Table 1
Summary of Mössbauer data of the compounds discussed in the text

Compound	$C_{11}H_9FeN$	*cis*-$C_{14}H_{10}FeN_2$	*trans*-$C_{14}H_{10}FeN_2$		$C_{15}H_9FeN_3$		*cis*-$C_{13}H_{10}FeIN$	*trans*-$C_{13}H_{10}FeIN$	Units
No.	**1**	**2**	**3**	**3**	**4**	**4**	**5**	**6**	
IS(90)	0.513(2)	0.516(9)	0.519(7)	0.527(8)	0.522(6)	0.525(5)	0.541(3)	0.551(2)	mm s^{-1}
IS(DFT)	0.492	0.467	0.509		0.489		0.463	0.398	mm s^{-1}
QS(90)	2.390(2)	2.226(9)	2.324(23)	2.114(26)	2.203(15)	1.902(14)	2.261(3)	2.240(2)	mm s^{-1}
QS(DFT)	2.283	2.241	2.300		2.147		2.310	2.237	mm s^{-1}
d IS/dT	4.08(2)	4.00(33)	4.53(11)	4.01(2)	4.21(8)	4.14(8)	4.28(2)	4.03(2)	(mm s^{-1} K) × 10^{-4}
$-\ln A$/dT	curv.	6.34(44)			5.69(12)		7.58(30)	6.48(9)	K^{-1} × 10^{-3}
M_{eff}	102(1)	104(8)			117 (ave)		97(4)	103(1)	Da

QS over the interval $95 < T < 297$ K. In the present case, the temperature dependence of IS is given by $\mathrm{d\,IS/d}T = -(4.00 \pm 0.33) \times 10^{-4}$ mm s^{-1} K^{-1} with a correlation coefficient of 0.995 for 12 data points. As above, this linearity leads to a value $M_{\mathrm{eff}} = 104 \pm 8$ Da in good agreement with the value for **1**. In contrast to the monocyano compound, here the $\ln A$ data, too, are well fitted by a linear regression and evidence a slope of $-(6.34 \pm 0.44) \times 10^{-3}$ K^{-1}, with a correlation coefficient of 0.994 for 12 data points. This temperature dependence, in conjunction with the $\mathrm{d\,IS/d}T$ value leads to a calculated Mössbauer lattice temperature, $\Theta_{\mathrm{M}} = 108$ K, justifying the "high temperature" limiting slope calculation inherent in the calculation of Θ_{M}. The single crystal X-ray diffraction data for **2** have been determined by Nemykin et al. [8] at 293 K. From their $U_{i,j}$ values it is possible to calculate the mean square amplitude of vibration (msav) of the metal atom. This quantity can also be derived from the temperature dependence of the area under the resonance curve observed in the ME spectra and leads to the dimensionless parameter $\mathscr{F} = -\ln f = k^2\langle x^2_{\mathrm{ave}}\rangle$, where f and k are as defined above. From the X-ray data at 293 K. $\mathscr{F}_{x,293}$ is 1.69(2), while the ME data yield a value of 1.86(13). It should also be noted that in the presence of lattice defects or crystal packing effects there may be a contribution to the X-ray $U_{i,j}$ values from these static positional distributions, although in molecular solids of the kind here considered these effects are usually negligibly small. In this model, the X-ray vibrational amplitudes will generally be equal to or larger than the values derived from the MES data at the same temperature. In the case of compound **2**, the two $\mathscr{F}$ values are within experimental error of each other, and the reasonable agreement between the two values is taken as validation of the model used in this analysis. In addition, it should be noted that the Glidewell et al. [22] X-ray data for **1** yield a value of 1.88 at 294 K in good agreement with the data for **2**.

As in the case of **1** the area ratio (**R**) is temperature independent within experimental error (±2%) again confirming the absence of a vibrational asymmetry of the iron atom. Despite the presence of two relatively large CN groups, there is no evidence here for the hydrogen bonding interaction noted by Glidewell et al. [22] since the nearest neighbor H–N distances at 293 K are 3.485 (H171–N17) and 4.198 (H151–N17) Å. Clearly the CN groups do not significantly interact with the *intra* molecular non-substituted ring of the molecule and thus do not contribute to the msav of the metal atom.

(c) *Compound* **3***:* Although at first glance the MES of **3** appear very similar to those of **1** and **2**, it was soon observed that the computer calculated line widths were noticeably broader than could be expected from sample thickness considerations. Consequently, these data were fitted to two distinct Fe sites, having similar but distinct IS and QS values, and a typical spectrum is shown in Fig. 2. This assumption leads to significantly better χ^2 values in the final fits and this fact is reflected in the two sets of IS values reported in Table 1. Reference to the 293 K X-ray diffraction values of Nemykin et al. [8] showed indeed that the site occupancy data for C8, C9, C10, N11 and N13, was 0.5 instead of unity, signifying disorder in the position of the cyano groups. The two configurations have slightly different IS values at all temperatures, as summarized graphically in Fig. 3, and the two temperature dependencies, $(-\mathrm{d\,IS/d}T)$, are $(4.53 \pm 0.11) \times 10^{-4}$ and $(4.01 \pm 0.20) \times 10^{-4}$ mm s^{-1} K^{-1}, respectively with correlation coefficients of 0.99 or better for 10 data points. In contrast, the QS values are essentially temperature independent within experimental error and differ by ~0.15 mm s^{-1} for the two configurations. As noted above, the recoil-free fraction data are well accounted for by a linear regression in the temperature

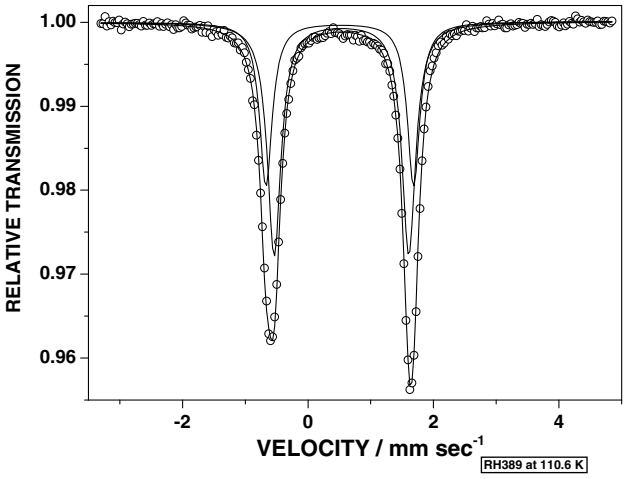

Fig. 2. ^{57}Fe Mössbauer spectrum of **3** at 110.6 K. The area ratio of the two subspectra is 0.83:1.0.

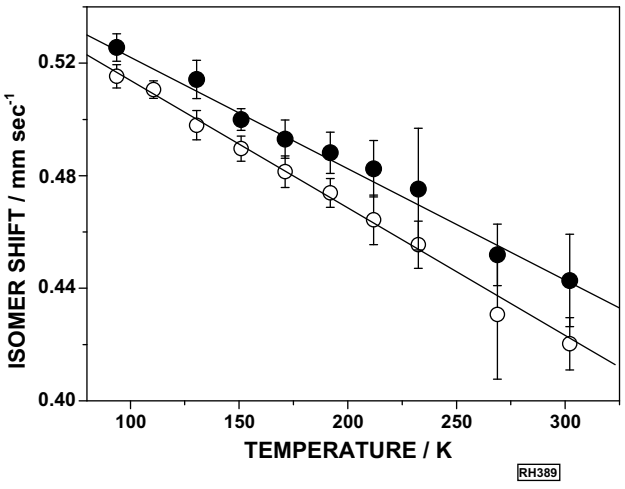

Fig. 3. Temperature dependence of the IS for the two sites observed for **3**. The full data points refer to the site with the smaller quadrupole splitting (see Fig. 2).

interval $171 < T < 302$ K, $-\mathrm{d}\ln A/\mathrm{d}T = (7.01 \pm 0.28) \times 10^{-3}\ \mathrm{K}^{-1}$ with a correlation coefficient of 0.997 for 6 data points. As above, this leads to a value of $\mathscr{F}_{\mathrm{M},293}$ of 1.28(7) from the low temperature MES data, and $\mathscr{F}_{x,293} = 1.87(4)$ from the X-ray diffraction $U_{i,j}$ values at 293 K.

(d) *Compound* **4***:* This compound has three cyano groups attached to the vinyl moiety and the ME spectra, like those of **3** are best fitted in terms of two slightly different configurations present in the solid state structure, having different hyperfine parameters in the range $94 < T < 294$ K. The single crystal X-ray data of Nemykin et al. [2] clearly show that the site occupancy factors of C7, C8, C9, C10, N12 and N14 are 0.5 both at 173 and 293 K with R_{F} factors of 0.0625 and 0.0324, respectively. The hyperfine parameters and derived constants are summarized in Table 1. The temperature dependence of the recoil-free fraction, f, is well fitted over the entire temperature range by a linear regression, and corresponds to a slope $-\mathrm{d}\ln A/\mathrm{d}T = (5.69 \pm 0.12) \times 10^{-3}\ \mathrm{K}^{-1}$ with a correlation coefficient of 0.998 for 11 data points. As pointed out above, this linearity permits the comparison of $\mathscr{F}$ between the X-ray and ME data at the two temperatures. These values at 173 and 293 K are $\mathscr{F}_{\mathrm{M},173} = 0.98(2)$ and $\mathscr{F}_{\mathrm{M},293} = 1.05(2)$ and $\mathscr{F}_{x,173} = 1.67(4)$ and $\mathscr{F}_{x,293} = 1.73(1)$ for the ME and X-ray data, respectively. In both cases the X-ray value is somewhat larger than the ME value as noted previously. Clearly the ME measurements give a reliable value for the msav of the metal atom in this compound. The temperature dependence of the IS is essentially the same for both configurations over the range $94 < T < 295$ K, and the average M_{eff} value for the two configurations is 100 ± 2 Da in reasonable agreement with the values obtained for the related compounds in this series. In other words, as noted earlier [24], changes in the ring substituents have only a very minor effect on the dynamical properties of the iron atom in such ferrocenoid structures. The Mössbauer lattice temperature, Θ_{M}, is 117 K. Finally, it is again worth noting that the area ratio of the two sites is essentially temperature independent over the noted temperature range, and has a value of 1.02 ± 0.08, indicating equal occupancy of the two configurations as noted in the X-ray study at 293 K.

(e) *Compound* **5***:* A persuasively convincing example of the validity of the above analysis of the metal atom dynamic data is provided by the equi-molecular weight compounds **5** and **6**. Compound **5** is the *cis* partner of the 1-iodo-2-cyano vinyl ferrocene pair and was examined over the temperature range $96 < T < 305$ K. The hyperfine and derived parameters are summarized in Table 1, from which it is noted that both iodo complexes have a somewhat larger IS at 90 K than the remainder of the cyano ferrocenes, but the temperature dependence of this parameter is comparable to the other values observed, leading to a normal effective vibrating mass, M_{eff}, associated with this type of complex. It is particularly noteworthy that the temperature dependence of the recoil-free fraction is well fitted over the temperature range up to 281 K with a correlation coefficient of 0.999 for 10 data points. A plot of this dependence is included in the data summarized in Fig. 4. As already noted, from this observation it is possible to calculate a value for the rms amplitude of vibration of the metal atom, as will be discussed in further detail, below. The QS parameter for **5** shows the expected negative dependence on temperature, and is not otherwise remarkable. There is no significant evidence for anisotropy of the metal atom motion over the indicated temperature range. The $\mathscr{F}$ values for **5** are $\mathscr{F}_{x,293} = 2.32(2)$ and $\mathscr{F}_{\mathrm{M},293} = 2.22(9)$ in good agreement with each other.

(f) *Compound* **6***:* The *trans* homologue of **5** was studied over the extended temperature range $93 < T < 336$ K and gave ME spectra consisting of narrow line doublets as noted above. The temperature dependence of the IS is not quite linear over the above range, but a linear fit to 15 data points evidenced a slope $-\mathrm{d}\,\mathrm{IS}/\mathrm{d}T = (4.032 \pm 0.024) \times 10^{-4}\ \mathrm{mm\ s^{-1}\ K^{-1}}$ with a correlation coefficient of 0.997. The M_{eff} value calculated from this slope is 103 ± 1 Da. The QS shows a normal decrease with increasing temperature, presumably due to cubic thermal expansion of the unit cell. The recoil-free fraction data shows some curvature especially in the high temperature region, but the lower temperature data ($93 < T < 305$ K) can be well fitted with a linear regression and yields a slope of $(6.48 \pm 0.08) \times 10^{-3}\ \mathrm{K}^{-1}$ with a correlation coefficient of 0.999 for 9 data points. This temperature dependence is again summarized in Fig. 4. The area ratio R has a value of 1.026 ± 0.008 over the range $153 < T < 336$ K, indicating largely isotropic amplitudes of vibration relative to the local symmetry axis running through the metal atom and consistent with the isotropic $U_{i,j}$ values at 293 K reported in the crystal structure data.

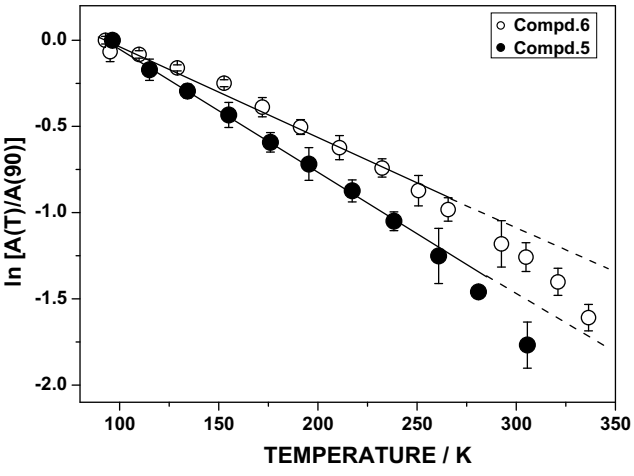

Fig. 4. Comparison of the temperature dependencies of the recoil-free fraction for **5** and **6**.

(g) *Comparison of the rmsav data for* **5** *and* **6***:* For **5**, the $k^2\langle x^2_{ave}\rangle$ values calculated from the X-ray data and the MES data at 293 K are 2.32(2) and 2.22(9), respectively, as already noted above, and this difference is presumably associated with the two types of vibrational motions present in molecular solids. As noted by Dunitz [25] in some of these cases the poor agreement between observed and calculated values of $U_{i,j}$ can plausibly be ascribed to internal molecular motions that invalidate the rigid body assumption, and it is this effect that appears to be operative in the case of compound **5**. A comparable calculation for **6** at 293 K leads to values of $\mathscr{F}_{x,293}$ of 1.98(3) and $\mathscr{F}_{M,293}$ of 1.90(3) for the X-ray and MES data, respectively. For compounds **5** and **6** the ratio of these parameters is 1.17 for the X-ray data and 1.16 for the MES data, in good agreement with each other. From this agreement it is useful to calculate the rmsav of the iron atom in those compounds where a linear $\ln A$ fit is obtained, and such a calculation for compounds **2, 4, 5** and **6** is summarized in Table 2. It is worth noting that as noted above, the recoil-free fraction data for **6** (but not for **5**) shows some curvature in the high temperature end of the dataset. The MES data related to the recoil-free fraction is assumed to be made up of the two major contributions: the molecular vibrations populated principally at low temperatures, and in addition the local atomic vibrations which become increasingly populated as T is increased. In making a linear regression to the data at low temperatures it has been assumed that in this regime the contribution of atomic motions contributes only in a minor way to the dynamics of the iron atom in these compounds, although as noted above, low frequency ring rotations and liberations can be populated even at relatively modest temperatures.

Table 1 (and Supporting Information Table 1) list values for DFT calculated components, V_{xx}, V_{yy}, and V_{zz} of the electric field gradient tensor, the asymmetry parameters, η, the quadrupole splittings, electron densities at the ^{57}Fe nucleus, and the isomer shifts calculated for compounds **1**–**6**. Except for **5** and **6** the QS parameters are essentially temperature independent over the range $90 < T < 300$ K. and even for **5** and **6** this correction is only $\sim$0.02 mm s^{-1}, so that the values calculated from the DFT considerations and those derived from the ME data at 90 K are directly comparable. There is a very good agreement between theory and experiment for quadrupole splittings and isomer shifts for compound **1**, **2**, **5**, and **6**. However, in the case of compounds **3** and **4**, crystal packing forces create molecular disorder in the crystal resulting in two sets of quadrupole doublets with different quadrupole splitting and isomer shift parameters, and due to the inherent nature of the phase involved in the DFT calculations (gas phase), this disorder cannot be modeled. However, DFT calculations do agree to a greater extent with only one of the two different iron centers in both compounds **3** and **4**. Let $\mathbf{3}_1$ and $\mathbf{3}_2$ be representations of iron centers in two positional lattice isomers for compound **3**. Then, center $\mathbf{3}_1$ and center $\mathbf{3}_2$ have isomer shift and quadrupole splitting parameters of 0.519 and 0.527 mm s^{-1} and 2.324 and 2.114 mm s^{-1}, respectively. DFT predicts an isomer shift and quadrupole splitting of 0.509 and 2.300 mm s^{-1}, respectively, which are much closer to the parameters pertaining to center $\mathbf{3}_1$. Similarly, let $\mathbf{4}_1$ and $\mathbf{4}_2$ be representations of iron centers in two positional lattice isomers for compound **4**. Then, center $\mathbf{4}_1$ and center $\mathbf{4}_2$ have isomer shift and quadrupole splitting parameters of 0.522 and 0.525 mm s^{-1} and 2.203 and 1.902 mm s^{-1}, respectively. DFT predicts an isomer shift and quadrupole splitting of 0.489 and 2.147 mm s^{-1}, respectively, which are much closer to parameters pertaining to center $\mathbf{4}_1$. Also, it has been determined that increasing the number of cyano groups attached to the vinyl ligand has only a minor effect on the s-electron density at the Fe nucleus in compounds **1**–**6** and thus it is difficult to extract such clear trends in the calculated quadrupole splittings and isomer shifts.

Table 2
Root-mean-square-amplitudes-of-vibration (rmsav) of the metal atom in several of the compounds discussed in the text

Compound	2	4	5	6	Units
Correl. coeff. (K)	0.994 (12)	0.006 (11)	0.9995 (10)	0.999 (9)	[a]
100	0.109	0.104	0.118	0.110	Å
150	0.133	0.128	0.144	0.135	Å
200	0.154	0.147	0.167	0.156	Å
250	0.172	0.156	0.186	0.174	Å
300	0.188	0.181	0.204	0.191	Å

[a] The number in parentheses indicates the number of different temperature points included in the linear correlation.

4. Summary and conclusions

Both temperature-dependent ^{57}Fe Mössbauer effect spectroscopy and density functional theory calculations have been used to elucidate the hyperfine interaction parameters of a number of structurally related cyano ferrocene complexes. The MES data related to the temperature dependence of the recoil-free faction, f, over the range $90 < T < 300$ K have been used to calculate the mean square amplitudes of vibration of the metal atom in these complexes. The availability of single crystal X-ray diffraction data for these compounds has afforded a comparison between the vibrational amplitudes derived from the MES data and the X-ray results, and the comparison provides an insight into the contributions of local high frequency (atomic) and low frequency (molecular) modes to the dynamics of the Fe atom. A comparison between the DFT calculation results and the data derived from the MES measurements are in very good agreement with each other and lead to a better understanding of the factors influencing the magnitude and symmetry of the charge distribution around the metal center. The presence at high temperatures of two nearly equivalent configurations of

compound **3** suggested in the X-ray data has been confirmed by the MES results. A comparison of the parameters for the *cis* and *trans* isomers of the iodo cyano complexes, **5** and **6** is also reported.

Acknowledgements

Generous support from the Research Corporation (Cottrell College Science Award CC6766, University of Minnesota Grant-in-Aid (Grant 20209) and Minnesota Supercomputing Institute to VN, as well as University of Minnesota Duluth Undergraduate Research Opportunity Grants to J.G. and RH (U. of M.) are greatly appreciated.

Appendix A. Supplementary material

Supplementary data associated with this article can be found, in the online version, at doi:10.1016/j.jorganchem.2008.02.010.

References

[1] M.C. Hodgson, A.K. Burrell, P.D.W. Boyd, P.J. Brothers, C.E.F. Rickard, J. Porph. Phthalocyan. 6 (2002) 737–747;
Z. Jin, K. Nolan, C.R. McArthur, A.B.P. Lever, C.C. Leznoff, J. Organomet. Chem. 468 (1994) 205–212;
K.-W. Poon, W. Liu, P.-K. Chan, Q. Yang, T.-W.D. Chan, T.C.W. Mak, D.K.P. Ng, J. Org. Chem. 66 (2001) 1553–1559;
V.N. Nemykin, N. Kobayashi, Chem. Commun. (2001) 165–166;
V.N. Nemykin, C.D. Barrett, R.G. Hadt, R.I. Subbotin, A.Y. Maximov, E.V. Polshin, A.Y. Koposov, Dalton Trans. (2007) 3378–3389.
[2] V.N. Nemykin, A.Y. Maximov, A.Y. Koposov, Organometallics 26 (2007) 3138–3148.
[3] R.H. Herber, I. Nowik, Hyperfine Int. 166 (2005) 351–355.
[4] R.H. Herber, I. Nowik, V. Kahlenberg, H. Kopacka, H. Schottenberger, Eur. J. Inorg. Chem. (2006) 3255–3260.
[5] R.H. Herber, A.R. Kudinov, P. Zanello, I. Nowik, D.S. Perekalin, V.I. Menscheryakov, K.A. Lyssenko, M. Corsini, S. Fedi, Eur. J. Inorg. Chem. (2006) 1786–1795.
[6] R.H. Herber, I. Nowik, Y. Matsuo, M. Toganoh, Y. Kuninobu, E. Nakamura, Inorg. Chem. 44 (2005) 5629–5635.
[7] A. Kivrak, M. Zora, J. Organomet. Chem. 692 (2007) 2346–2349.
[8] V.N. Nemykin, E.A. Makarova, J.O. Grosland, R.G. Hadt, A.Y. Koposov, Inorg. Chem. 46 (23) (2007) 9591–9601.
[9] M. Glaberson, M. Brettschneider; see <www.PHYS.HUJI.AC.IL~glabersn>.
[10] M.J. Frisch, G.W. Trucks, H.B. Schlegel, G.E. Scuseria, M.A. Robb, J.R. Cheeseman, J.A. Montgomery, Jr., T. Vreven, K.N. Kudin, J.C. Burant, J.M. Milam, S.S. Iyengar, J. Tomasi, V. Barone, B. Mennucci, M. Cossi, G. Scalmani, N. Rega, G.A. Petersson, H. Nakatsuji, M. Hada, M. Ehara, K. Toyota, R. Fukuda, J. Hasegawa, M. Ishida, T. Nakajima, Y. Honda, O. Kitao, H. Nakai, M. Klene, X. Li, J.E. Knox, H.P. Hratchian, J.B. Cross, C. Adamo, J. Jaramillo, R. Gomperts, R.E. Stratmann, O. Yazyev, A.J. Austin, R. Cammi, C. Pomelli, J.W. Ochterski, P.Y. Ayala, K. Morokuma, G.A. Voth, P. Salvador, J.J. Dannenberg, V.G. Zakrzewski, S. Dapprich, A.D. Daniels, M.C. Strain, O. Farkas, D.K. Malick, A.D. Rabuck, K. Raghavachari, J.B. Foresman, J.V. Ortiz, Q. Cui, A.G. Baboul, S. Clifford, J. Cioslowski, B.B. Stefanov, G. Liu, A. Liashenko, P. Piskorz, I. Komaromi, R.L. Martin, D.J. Fox, T. Keith, M.A. Al-Laham, C.Y. Peng, A. Nanayakkara, M. Challacombe, P.M.W. Gill, B. Johnson, W. Chen, M.W. Wong, C. Gonzalez, J.A. Pople, GAUSSIAN 03, Revision C.02; Gaussian, Inc., Wallingford CT, 2004.
[11] A.D. Becke, Phys. Rev. A 38 (1988) 3098–3100.
[12] J.P. Perdew, Y. Wang, Phys. Rev. B 45 (1992) 13244–13249.
[13] A.J.H. Wachters, J. Chem. Phys. 52 (1970) 1033–1036.
[14] (a) F. Biegler-Konig, AIM2000, version 1.0; University of Applied Science: Bielefeld, Germany;
(b) R.F.W. Bader, Atoms in Molecules A Quantum Theory, Oxford University Press, Oxford, 1990.
[15] V.I. Goldanskii, E.F. Makarov, in: V.I. Goldanskii, R.H. Herber (Eds.), Chemical Applications of Mössbauer Spectroscopy, Academic Press Inc., New York, 1968, pp. 46 ff–60 ff, See also N.N. Greenwood, T.C. Gibb in Mössbauer Spectroscopy Chapman Hall Ltd., London, 1971, (Chapter 3).
[16] P. Gütlich, J. Ensling, in: A.B.P. Lever, E.I. Solomon (Eds.), Inorganic Electronic Structure and Spectroscopy, vol. I, John Wiley & Sons, New York, 1999, pp. 161–212.
[17] V.N. Nemykin, R.G. Hadt, Inorg. Chem. 45 (2006) 8297–8307.
[18] P. Dufek, P. Blaha, K. Schwarz, Phys. Rev. Lett. 75 (1995) 3545–3548.
[19] S. Sinnecker, L.D. Slep, E. Bill, F. Neese, Inorg. Chem. 44 (2005) 2245–2254.
[20] R.H. Herber, in: R.H. Herber (Ed.), Chemical Mössbauer Spectroscopy, Plenum Press, New York, 1984, p. 210.
[21] V.I. Gol'danskii, E.F. Makarov, in: V.I. Gol'danskii, R.H. Herber (Eds.), Chemical Applications of Mössbauer Spectroscopy, Academic Press, New York, 1968, p. 37.
[22] W. Bell, G. Ferguson, C. Glidewell, Acta Crystallogr., Sect. C 52 (1996) 1928–1930.
[23] (a) V.I. Gol'danskii, G.M. Gorodinskii, S.V. Karyagin, L.A. Korytko, L.M. Khrizhanskii, E.F. Makarov, I.P. Suzdalev, V.V. Khrapov, Doklady Akad. Nauk SSSR 147 (1962) 127;
(b) S.V. Karyagin, Doklady Akad. Nauk SSSR 148 (1963) 1102.
[24] (a) I. Nowik, M. Wagner, R.H. Herber, J. Organomet. Chem. 688 (2003) 11–14;
(b) R.H. Herber, I. Nowik, D.A. Loginov, Z.A. Starikova, A.R. Kudinov, Eur. J. Inorg. Chem. (2004) 3476–3483.
[25] J.D. Dunitz, X-ray Analysis and the Structure of Molecules, Cornell University Press, Ithaca, 1979, p. 257.